ACS Sustainable Chemistry & Engineering

October 7, 2019 | Volume 7 Number 19

pubs.acs.org/acssce

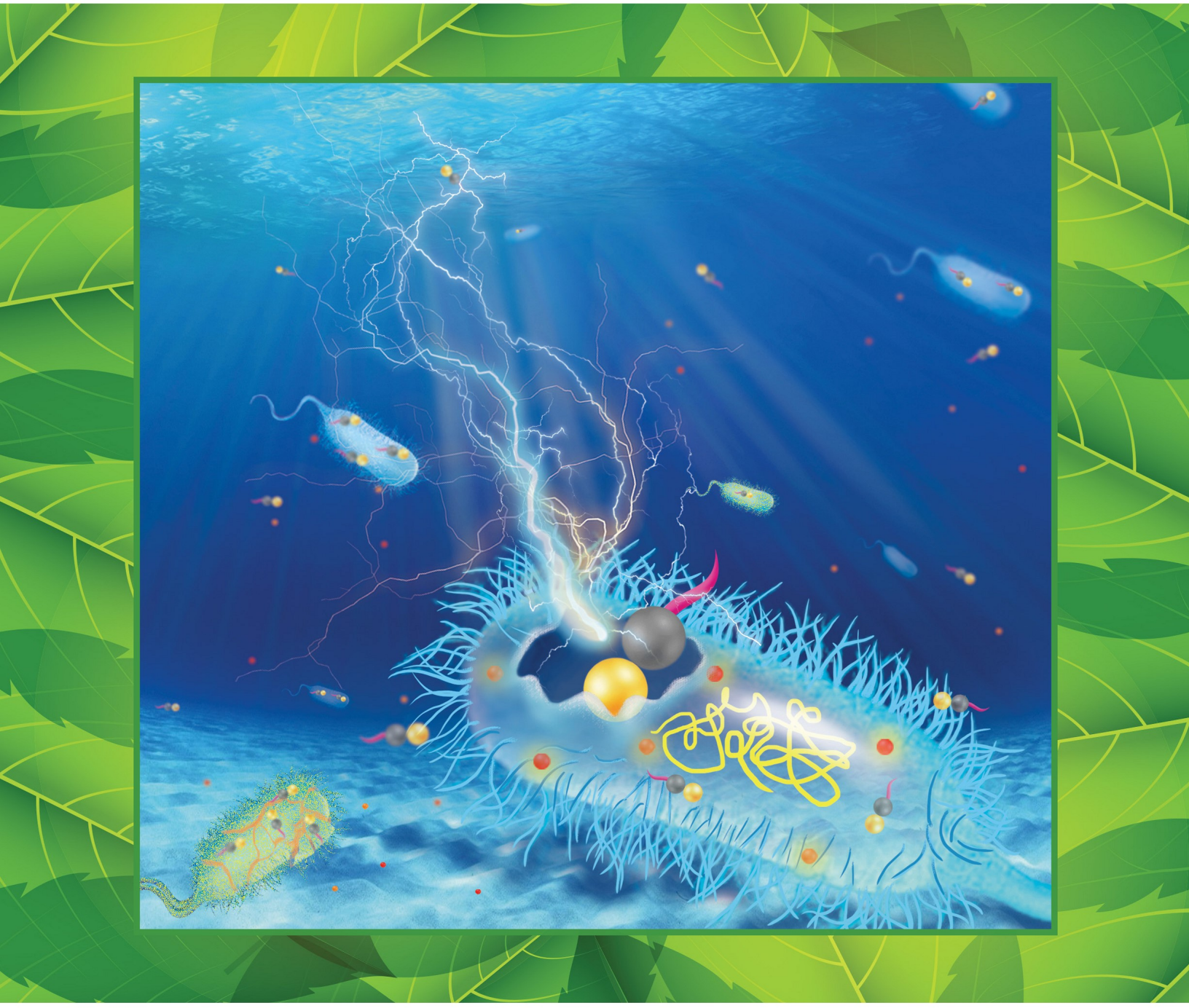

ACS Publications
Most Trusted. Most Cited. Most Read.

www.acs.org

ACS Sustainable Chemistry & Engineering

Research Article

Cite This: ACS Sustainable Chem. Eng. 2019, 7, 16264−16273

pubs.acs.org/journal/ascecg

Antimicrobial Activity of Zinc Oxide−Graphene Quantum Dot Nanocomposites: Enhanced Adsorption on Bacterial Cells by Cationic Capping Polymers

Junli Liu,*[,†,‡] Jianzhen Shao,[†,‡] Yuhan Wang,[†,‡] Junqi Li,[†,‡] Hui Liu,[†,‡] Aiqin Wang,[§] Aiping Hui,[§] and Shaowei Chen*[,∥]

[†]School of Materials Science and Engineering, and [‡]Shaanxi Key Laboratory of Green Preparation and Functionalization for Inorganic Materials, Shaanxi University of Science & Technology, Weiyang University Park, Xi'an 710021, China

[§]Key Laboratory of Clay Mineral Applied Research of Gansu Province, Center of Eco-material and Green Chemistry, Lanzhou Institute of Chemical Physics, Chinese Academy of Sciences, 18 Tianshui Middle Road, Lanzhou 730000, China

[∥]Department of Chemistry and Biochemistry, University of California, 1156 High Street, Santa Cruz, California 96064, United States

Supporting Information

ABSTRACT: Development of low-cost, high-performance antibacterial reagents is of critical importance in the face of increasing occurrence of bacterial resistance against conventional antibiotics. In the present study, polyethylenimine (PEI)-modified graphene quantum dot (GQD) and ZnO nanoparticle nanocomposites, which were readily dispersed in water and exhibited markedly enhanced antimicrobial activity toward *Escherichia coli*, as compared to the PEI-free ZnO/GQD counterparts, were prepared by a facile sol−gel method. This was largely ascribed to the reduced size of the nanoparticles and the enhanced adsorption of the nanocomposites onto the bacterial cell surfaces, as manifested by adsorption experiments and TEM characterization of the bacterial cells, as well as electron spin resonance measurements. The results highlight the significance of structural engineering of functional nanocomposites in the development of efficient antibacterial agents.

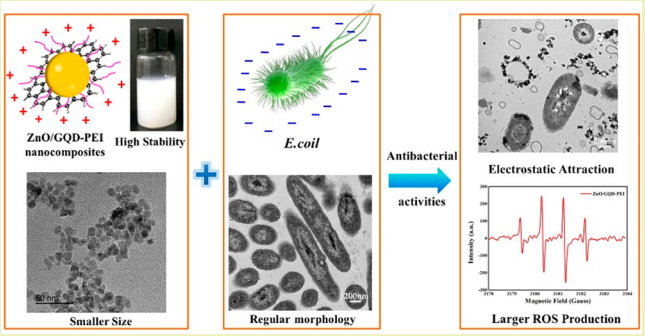

KEYWORDS: *Zinc oxide, Graphene quantum dot, Polyethylenimine, Electrostatic interaction, Surface adsorption, Antibacterial activity*

INTRODUCTION

Bacterial infectious diseases, especially the increasing occurrence of "superbugs", have become a serious threat to human health.[1,2] Traditional treatment strategies involve chlorination, ozone, ultraviolet radiation, and the use of organic antibacterial agents, yet these are usually carcinogenic, expensive, and/or eco-unfriendly.[3−5] In recent decades, the emergence and rapid progress of nanotechnology has enabled the development of novel, potent antibacterial reagents based on inorganic nanomaterials that possess unique physical and chemical characteristics to overcome the bacterial drug resistance but with minimal impacts on the environment.[6] Among these, metal oxide nanoparticles, such as ZnO,[7,8] TiO_2,[9−11] and BiOI,[12,13] have been used as low-cost, effective antibacterial reagents. In addition, nanoparticles of copper,[14] silver,[15] zinc,[16] and magnesium[17] have also been found to exhibit apparent antimicrobial activity. In these studies, the antibacterial activity has been observed to vary with the sizes and morphologies of the nanomaterials.[18−20] Nanoparticles with a reduced size can easily absorb on the surface of bacterial cells, damaging cell membranes, as well as DNA structures,[17] and thus exhibit outstanding antibacterial activity.[21] For instance, Applerot et al.[22] showed that the growth rates of *Escherichia coli* and *Staphylococcus aureus* were reduced by 99.8% and 98%, respectively, when they were treated with ZnO nanoparticles (6.8 nm in diameter) at the concentration of 0.1 mg/L. Li et al.[23] prepared composite films based on CdTe quantum dots (QDs) and poly-L-lysine (PLL) and demonstrated that the antibacterial activity was largely dictated by CdTe QDs, which increased with an increasing loading of the QDs. Hui et al.[13] prepared open-caged C60 and observed bactericidal activity specifically against *S. aureus*, but not *Bacillus subtilis*, *Pseudomonas aeruginosa*, or *E. coli*, which was accounted for by the matching surface morphology that facilitated the adsorption of C60 onto the bacterial cell surface and hence disruption of the cell envelope. Stankovic et al.[24] prepared thin

Received: June 10, 2019
Revised: July 25, 2019
Published: August 9, 2019

DOI: 10.1021/acssuschemeng.9b03292
ACS Sustainable Chem. Eng. 2019, 7, 16264−16273

films of carbon nanodots and observed that the antibacterial activity could be enhanced by blue light photoirradiation, due to the production of singlet oxygen that attacked the cell membrane, increased its porosity, and allowed radical species to reach the cytoplasmic membrane and eventually damage the cells. In our recent study,[25] composites (diameter 30−40 nm) based on ZnO nanoparticles and graphene quantum dots (GQD), synthesized via a simple hydrothermal technique, were readily dispersible in water, in contrast to results in earlier studies where the nanoparticles were substantially larger and insoluble in water. Remarkably, the nanocomposites exhibited excellent photoenhanced antibacterial activity, which was attributed to the effective interfacial charge transfer from GQD to ZnO that accelerated the generation of reactive oxygen species (ROS) under photoirradiation. One immediate question arises: Will the activity be further improved by a reduction of the size and structure of the nanocomposites and by enhanced adsorption of the nanocomposites onto the bacterial cells? Previous studies have shown that electrostatic interactions between nanocomposites and bacterial cells play a vital role in the antibacterial effect. For instance, Stoimenov et al.[26] reported that the electrostatic interactions of MgO nanoparticles with bacterial surfaces could be exploited for enhanced antibacterial activity. An et al.[27] demonstrated that Mg^{2+}-modified zeolite exhibited much stronger adsorption and higher affinity toward *E. coli* than pristine zeolites. Zemb et al.[28] observed that the addition of sodium chloride to freshwater or dilute mineral salt medium increased the adsorption of T2 phages on *E. coli*.

In the present study, water-soluble nanocomposites based on PEI-functionalized GQD (GQD−PEI) and ZnO nanoparticles were prepared. TEM measurements showed that the resulting ZnO/GQD−PEI nanocomposites exhibited a markedly reduced diameter of 12−16 nm, and significantly improved antibacterial activity against *E. coli*, in comparison to the ZnO/GQD counterpart. Experimentally, the ZnO/GQD−PEI nanocomposites exhibited a low minimum inhibition concentration (MIC) of only 2.0 mg/mL, which was evidently superior to that of the ZnO/GQD nanocomposites (4.0 mg/mL). The enhanced antibacterial activity was largely ascribed to the enhanced absorption of ZnO/GQD−PEI to the bacterial cells and ROS production by the ZnO/GQD−PEI nanocomposites, as manifested in electron microscopic, optical absorption, and electron spin resonance (ESR) measurements.

EXPERIMENTAL SECTION

Chemicals. Zinc acetate dihydrate [$Zn(OAc)_2{\cdot}2H_2O$], potassium hydroxide (KOH), citric acid, and absolute ethanol were all purchased from Tianjing Hongyan Chemical Regents Co., Ltd. Polyethylenimine (PEI, 99%, 1.8 kDa) and 1-(3-(dimethylamino)propyl)-3-ethylcarbodiimide hydrochloride (EDC·HCl) were obtained from Macklin Biochemicals Co., Ltd. All chemicals were of analytic reagent grade and used directly without further treatment. Water was supplied with a Barnstead Nanopure Water System (18.3 MΩ cm).

Preparation of Graphene Quantum Dots (GQDs). GQDs were synthesized by pyrolysis of citric acid at 200 °C, as described previously.[29] GQD−PEI was also prepared by adopting a previous method with minor modifications.[30] In a typical experiment, 0.1 g of PEI was added into a diluted dispersion of GQDs (100 mL, 1 mg/mL) under sonication for 10 min, into which was then added 0.382 g of EDC·HCl with magnetic stirring for 24 h. The mixture was dialyzed in Nanopure water for 1 day with frequent changes of water, and the purified sample is denoted as GQD−PEI(1×).

Five more GQD−PEI samples were prepared in the same fashion except that the initial loading of PEI was increased to 0.2, 0.4, 0.6, 0.8, and 1.0 g, along with a proportional increase of the amount of EDC·HCl added. The corresponding samples are referred to as GQD−PEI(2×), GQD−PEI(4×), GQD−PEI(6×), GQD−PEI(8×), and GQD−PEI(10×), respectively.

Synthesis of ZnO/GQD−PEI Nanocomposites. The ZnO/GQD−PEI nanocomposites were synthesized by following a sol−gel process with slight modifications.[30,31] Briefly, $Zn(OAc)_2{\cdot}2H_2O$ (0.98 g) and KOH (0.486 g) were dispersed in 100 and 50 mL of ethanol, respectively. Then, 50 mg of the GQD−PEI prepared above was slowly dispersed into the $Zn(OAc)_2$ solution under sonication, into which was then added the KOH solution in a dropwise fashion under magnetic stirring. The resulting solution was homogenized by constant stirring and heated at 95 °C for 5 h, before the precipitates were collected by centrifugation, washed with deionized water and ethanol, and dispersed in water. ZnO/GQD nanocomposites were prepared in the same fashion but using an equivalent amount of GQD instead of GQD−PEI.

Characterization. X-ray diffraction (XRD) measurements were carried out with a Rigaku D/MAX-2200 diffractometer with Co Kα radiation (λ = 0.179 nm). TEM studies were carried out with a Tecnai G2 F20 S-TWIN microscope at the accelerating voltage of 200 kV. FTIR spectra were acquired with an AECTOR-22 spectrometer. X-ray photoelectron spectroscopy (XPS) analysis was performed with an AXIS SUPRA spectrometer, using carbon (C 1s binding energy 284.6 eV) as the calibration reference. ESR measurements were performed with a JEOL JES-FA200 instrument at room temperature using 5-dimethylpyrroline 1-oxide (DMPO) as the spin -trapping agent. The ζ-potential was measured by a Malvern Nano-ZS powder particle size analyzer at room temperature, where samples at the same concentration and *E. coli* (optical density, OD = 0.1) were dispersed in deionized water. Thermogravimetric analysis (TGA) was conducted using a STA409PC thermogravimetric analyzer at the heating rate of 5 °C/min.

Minimum Inhibitory Concentration (MIC) Experiments. The tested bacteria were inoculated in 96-well plates with the above-obtained nanocomposites at different concentrations and sterile liquid medium. Then, the plates were immediately placed into a Molecular Devices SpectraMax Plus Microplate reader, where the OD at 600 nm was measured every 10 min for 24 h at 37 °C.

Photodynamic Antibacterial Assessments. A 0.5 mL portion of the bacterial suspension was added to a 2 mL plastic centrifuge tube, into which was then added 0.5 mL of the above-obtained nanocomposites. After UV photoirradiation (100 W, Guangmingyuan Lighting Co.) for a select period of time, 20 μL of the bacterial suspension was swabbed uniformly onto a plate, which was incubated at 37 °C for 18 h before the survival cell percentage was calculated.

Cell Adsorption Test. One milligram of the nanocomposites prepared above was added to a 10 mL centrifuge tube that contained *E. coli* (OD = 0.1), and the mixture was placed in a shaking incubator at 200 rpm for 10 h at 4 °C. The sample was then collected by centrifugation at 3000 rpm for 10 min, and the OD of the supernatant (*E. coli* without absorbed nanocomposites) was measured with a UV−vis spectrophotometer.

TEM Characterization of Bacterial Cells. *E. coli* cells were inculcated with the nanocomposites prepared above (1 mg/mL) in accordance with the conditions for cell absorption experiments. Then, bacteria cells were collected by centrifugation and fixed with 2.5% glutaraldehyde and paraformaldehyde at 4 °C for 2 h. Thereafter, it was washed with a 0.1 M PBS solution for 30 min, postmixed with 1% osmic anhydride at 4 °C for 2 h, and washed with PBS again. Then, the cells were dehydrated with acetone solutions (30%, 50%, 70% for 10 min each, 90% for 10 min twice, and 100% for 10 min three times), and displaced by propylene epoxide. The bacterial cells were then embedded into EMbed 812 and DDSA resin, which was cut into ultrathin slices, colored by impregnation of citric acid, and examined by TEM measurements.

DOI: 10.1021/acssuschemeng.9b03292
ACS Sustainable Chem. Eng. 2019, 7, 16264−16273

RESULTS AND DISCUSSION

Structural Characterizations. Figure 1 shows the representative TEM images of the (a) ZnO/GQD and (b) ZnO/GQD−PEI(6×) nanocomposites. Both samples can be seen to consist of a large number of dark-contrast particles, which are most likely ZnO nanoparticles, situated onto a light-contrast background (i.e., GQD). As the surface of ZnO is positively charged[32] and GQD is negatively charged,[33] the electrostatic attraction led to the agglomeration of ZnO nanoparticles on GQD (Figure 1a). This is alleviated by the PEI capping layer on the GQD surface, leading to improved dispersion of the ZnO nanoparticles, as shown in Figure 1b. In high-resolution TEM measurements (Figure 1c,d), both nanocomposites exhibit two sets of lattice fringes. One shows an interplanar spacing of 0.34 nm that can be ascribed to the (002) plane of graphitic carbon (i.e., GQD),[34] while the other of 0.28 nm is corresponding to the (001) plane of ZnO.[35] This confirms the successful incorporation of ZnO and GQD in the nanocomposites. In addition, statistical analysis based on more than 100 nanoparticles showed that the ZnO/GQD nanocomposites are mostly within the range of 7−12 nm in diameter, with an average of 9.5 ± 1.87 nm (Figure 1e). For comparison, the ZnO/GQD−PEI nanocomposites are somewhat larger, within the range of 12−16 nm, averaging 12.83 ± 1.58 nm (Figure 1f). The stability of ZnO/GQD and ZnO/GQD−PEI nanocomposites in water is displayed and compared in Figure 1g. It can be seen that the apparent precipitation started to occur with the ZnO/GQD sample after 24 h, whereas the ZnO/GQD−PEI nanocomposites remained stable in dispersion even after 48 h, which, again, was most likely due to the PEI capping layer.

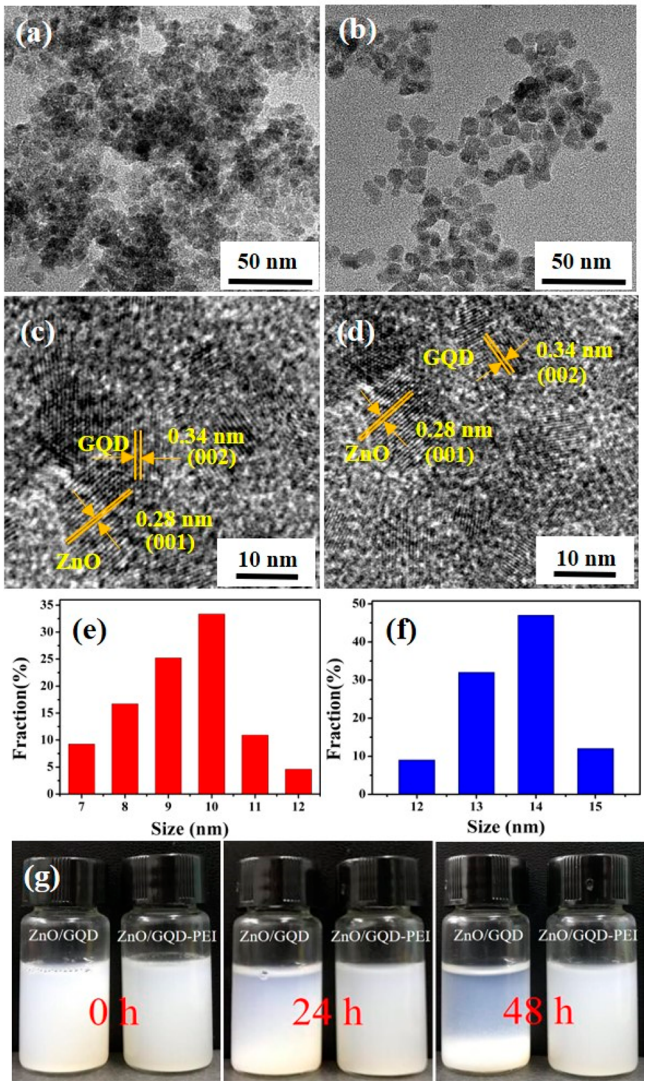

Figure 1. TEM images of (a, c) ZnO/GQD and (b, d) ZnO/GQD−PEI(6×) nanocomposites, with the corresponding size distributions shown in panels e and f, respectively. (g) Digital images of ZnO/GQD and ZnO/GQD−PEI(6×) nanocomposites after different storage times.

The sample structures were further characterized by XRD measurements. Figure 2 shows the XRD patterns of ZnO/GQD and ZnO/GQD−PEI(6×) nanocomposites. Both samples display a series of diffraction peaks at 2θ = 31.77°, 34.42°, 36.25°, 47.54°, 56.60°, and 62.86°, which can be attributed to the (100), (002), (101), (102), (110), and (103) planes of hexagonal wurtzite ZnO, respectively (JCPDS No. 36-1451).[36] Note that no diffraction features can be identified for GQD and PEI, because of their low contents and lack of crystallinity in the nanocomposites.[37]

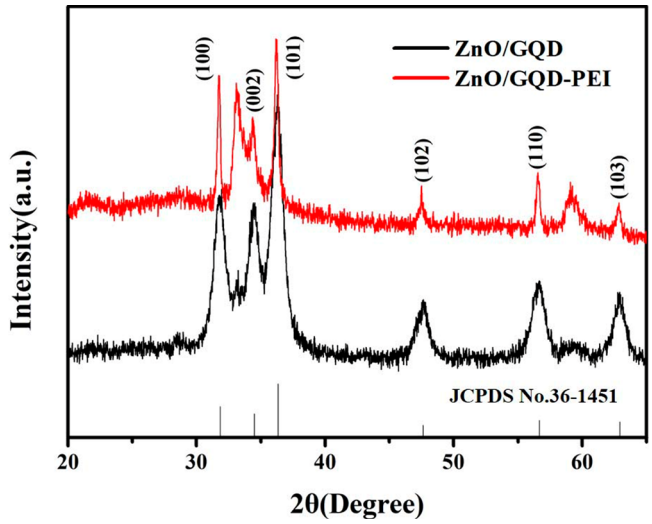

Figure 2. XRD patterns of ZnO/GQD and ZnO/GQD−PEI(6×) nanocomposites.

Additional structural insights were obtained in XPS measurements. Figure 3a shows the full survey spectra of ZnO/GQD and ZnO/GQD−PEI(6×) nanocomposites, where the elements of Zn, O, and C can be readily identified for both samples, and for ZnO/GQD−PEI(6×), N can also be found due to the PEI capping layer.[38] Figure 3b shows the high-resolution scans of the C 1s electrons of ZnO/GQD and ZnO/GQD−PEI(6×). In the latter, deconvolution yields four peaks at the binding energies of 284.60 eV for sp^2-hybridized C, 286.15 eV for C−O, 288.24 eV for C═O, and 285.10 eV for C−O−Zn,[39] at the atomic ratio of 14.1:4.4:1.0:5.4 [Table S1, Supporting Information (SI)]. In Figure 3c, the O 1s spectra can be seen to entail two subpeaks at the binding energies of 529.98 and 531.46 eV. The former is due to Zn−O−C,[39] and the latter to the carboxyl groups.[38,40] Figure 3d shows the corresponding Zn 2p scans, with Zn $2p_{3/2}$ at 1021.71 eV and Zn $2p_{1/2}$ at 1044.83 eV.[41] The N 1s scan of ZnO/GQD−PEI(6×) is depicted in Figure 3e, where two subpeaks can be

DOI: 10.1021/acssuschemeng.9b03292
ACS Sustainable Chem. Eng. 2019, 7, 16264−16273

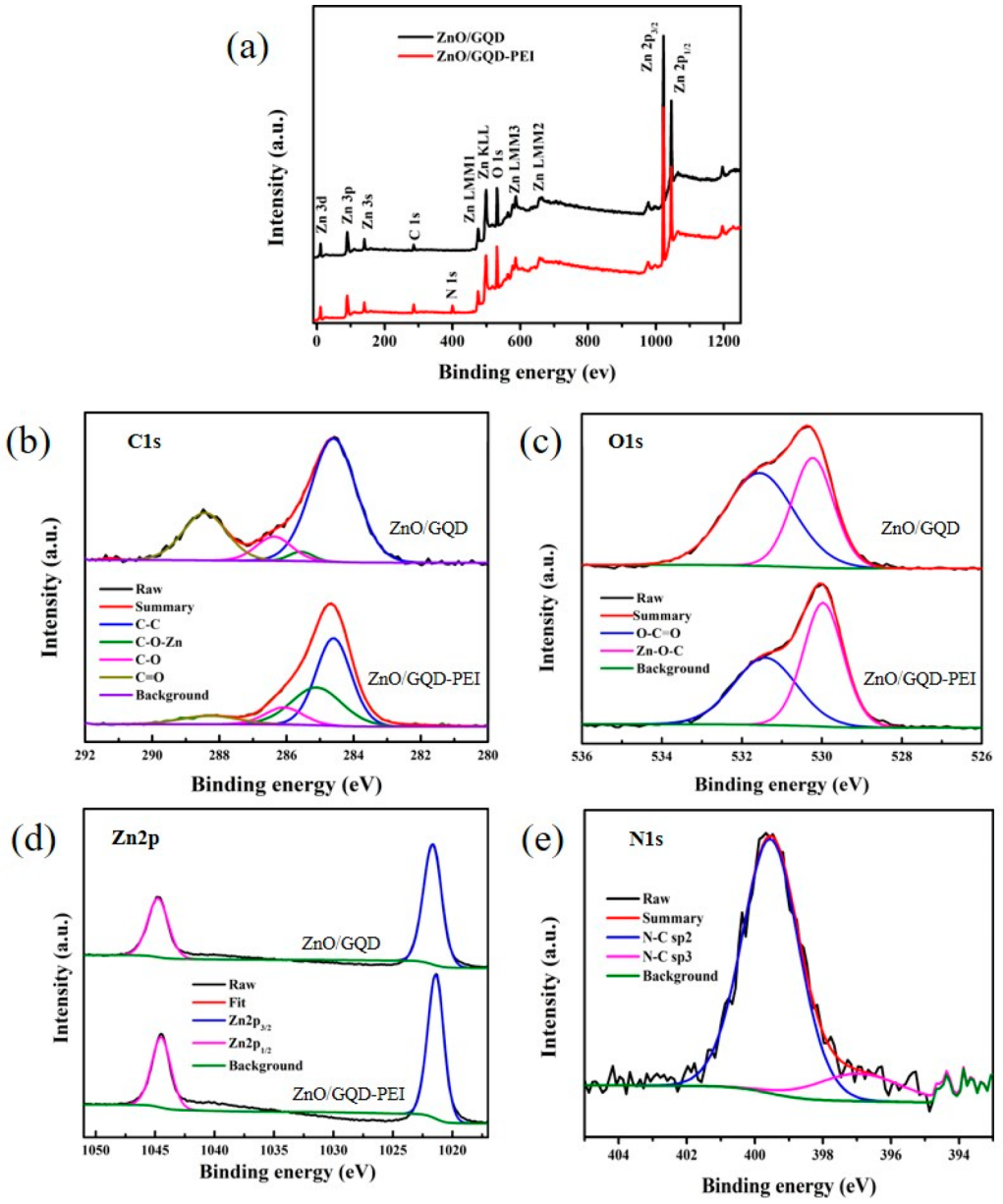

Figure 3. (a) XPS survey spectra of ZnO/GQD and ZnO/GQD−PEI(6×) nanocomposites, and high-resolution scans of the (b) C 1s, (c) O 1s, (d) Zn 2p, and (e) N 1s electrons.

resolved at 396.86 and 399.24 eV, due to C−N and C═N, respectively,[42] suggesting the formation of amide bonds in the composites. These results demonstrate that PEI was indeed successfully grafted with GQD, consistent with results obtained from FTIR measurements (Figure S1, SI).

TGA measurements were then carried out in order to quantify the content of PEI in ZnO/GQD−PEI(6×) nanocomposites. From Figure 4, it can be seen that the thermal decomposition of ZnO/GQD and ZnO/GQD−PEI(6×) nanocomposites involved two stages, with a total weight loss of 11.25% and 20.19%, respectively. For both samples, the first weight loss below 100 °C (about 2.5% and 3.35%) was most likely due to the evaporation of adsorbed water on the sample surfaces, and the second weight loss started at ca. 200 °C and ended at ca. 450 °C, where the GQD content was estimated to be 8.75% in ZnO/GQD and the PEI content 8.09% in ZnO/GQD−PEI.[43] That is, the weight ratio of GQD to PEI in the ZnO/GQD−PEI(6×) nanocomposite is about 1.08:1.

Note that the structural characteristics are very consistent with other samples in the series, except that the PEI content in the nanocomposites did increase somewhat with the initial feed loading of PEI. For instance, for the ZnO/GQD−PEI(1×) sample, the PEI content was 7.70%, only 0.39% lower than that in ZnO/GQD−PEI(6×).

Antibacterial Activity. The antimicrobial activity of the nanocomposites prepared above was then examined and compared by using *E. coli* as the example. Figure 5 displays the growth curves of *E. coli* in nutritional broth containing (a) ZnO/GQD and (b−g) ZnO/GQD−PEI nanocomposites at different concentrations under ambient conditions. It can be seen that, in comparison to the control sample, the growth of bacteria was markedly inhibited by both ZnO/GQD and ZnO/GQD−PEI nanocomposites. For instance, in the presence of 1.6 mg/mL ZnO/GQD nanocomposites, the bacterial growth was reduced by over 80%, as shown in Figure 5a. The inhibitory effect became intensified with an increasing

DOI: 10.1021/acssuschemeng.9b03292
ACS Sustainable Chem. Eng. 2019, 7, 16264−16273

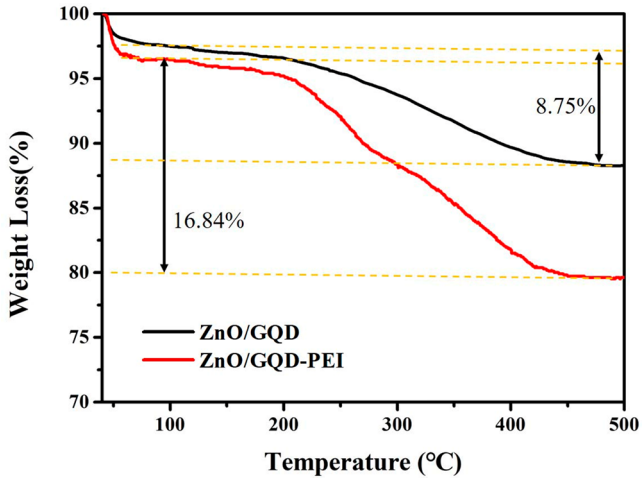

Figure 4. TGA curves of ZnO/GQD and ZnO/GQD−PEI(6×) nanocomposites.

concentration of the ZnO/GQD nanocomposites, and at the concentration of 4.0 mg/mL, virtually no bacterial growth was observed, suggesting that the MIC of ZnO/GQD is ca. 4.0 mg/mL. More effective inhibition was observed with the ZnO/GQD−PEI(1×) nanocomposite (Figure 5b), where only 0.9 mg/mL was needed to inhibit the bacterial growth by 80%, with a lower MIC of ca. 2.7 mg/mL. This might be attributed to the enhanced dispersion of ZnO/GQD−PEI nanocomposites, due to the incorporation of a PEI capping layer, that facilitates the interactions with the bacterial cells and hence antibacterial activity.[44] Moreover, the effects of PEI loading on the antibacterial activity of the ZnO/GQD−PEI composites were also investigated. Figure 5c−g shows the growth curves of *E. coli* cultured in a nutrient broth containing different ZnO/GQD−PEI nanocomposites for 24 h, where the MIC was estimated to be ca. 2.8 mg/mL for GQD−PEI(2×), 2.6 mg/mL for GQD−PEI(4×), 2.0 mg/mL for GQD−PEI(6×), 2.4 mg/mL for GQD−PEI(8×), and 2.7 mg/mL GQD−PEI(10×), respectively, all markedly lower than that of ZnO/GQD (4.0 mg/mL). These results confirmed that the antibacterial activity of ZnO/GQD−PEI nanocomposites to *E. coli* was greatly enhanced by surface modification of ZnO with cationic PEI polymers. Among the series, the ZnO/GQD−PEI(6×) nanocomposite exhibited the best antibacterial performance. This might be ascribed to the large difference between the ζ-potentials of ZnO/GQD−PEI(6×) nanocomposite (+16.67 mV) and *E. coli* (−25.7 mV) (Figure S2, SI), which led to strong absorption of the nanocomposites onto the bacterial cell surfaces and hence the antibacterial activity (vide infra).

The antimicrobial activity of the nanocomposites was then examined and compared under UV photoirradiation. On the basis of the above MIC results, the concentration of the nanocomposites was set at 2.0 mg/mL. The bacterial growth was quantified by counting the colony forming units (cfu). As depicted in Figure 6a, the survival percentage of *E. coli* depends strongly on the irradiation time and the specific nanocomposite samples. Specifically, under the treatment by ZnO/GQD and ZnO/GQD−PEI(6×) nanocomposites, the cfu decreased drastically with the prolongation of photoirradiation time, in contrast to the control experiment that remained almost invariant with time. The strong photoenhanced antibacterial activity is likely due to the increased production of ROS under UV photoirradiation, as observed previously.[25] Nevertheless, one can see that ZnO/GQD−PEI(6×) exhibited a higher activity than the PEI-free counterpart. For instance, only 3.1% of *E. coli* cells survived after the treatment of ZnO/GQD−PEI(6×) nanocomposite under UV irradiation for 5 min, while the percentage that survived was 40.7% with ZnO/GQD and 66.28% for the control. This is probably due to the synergistic interactions among the three constituents, where ZnO is the main antibacterial ingredient, GQD facilitates the effective charge transfer from GQD to ZnO, and PEI improves the dispersion of nanoparticles and contact efficiency between ZnO/GQD−PEI nanocomposites and *E. coli* cells. That is, cationic PEI facilitated the interaction with negatively charged bacterial cells, and the photochemical activity of ZnO and GQD led to damage and death of the bacteria.[44,45] Notably, the antibacterial activity can be further improved upon increasing the intensity of the UV photoirradiation (Figure S3, SI).

Antibacterial Mechanism. To verify the antibacterial mechanism of ZnO/GQD−PEI nanocomposites, ESR measurements were carried out to evaluate the production of ROS, and TEM studies were performed to examine the interaction between the nanocomposites and bacteria. Figure 7 displays the ESR spectra of blank water and aqueous solutions of ZnO/GQD and ZnO/GQD−PEI(6×) nanocomposites. DMPO was used as the spin trap for hydroxyl radicals ($^{\bullet}OH$). It can be seen that no obvious ESR signal was detected in the blank sample (black line). However, the addition of ZnO/GQD and ZnO/GQD−PEI(6×) nanocomposites resulted in the appearance of well-defined ESR signals (Figure 7), indicating that the formation of hydroxyl radicals was mainly due to the photochemical activity of ZnO/GQD. However, the signal intensity of the ZnO/GQD−PEI(6×) nanocomposite was much stronger than that of ZnO/GQD, suggesting an enhanced efficiency of ROS production by the former, likely due to electron transfer to ZnO/GQD particles from the $PEI^{\bullet}$ radical as well as PEI-derived amino radical ($NH_4^{\bullet}$).[46−48]

To quantify the adsorption of nanoparticles on the surface of *E. coli*, the dispersion was centrifuged and the supernatant was subject to optical absorption measurement, where the OD value represented the concentration of *E. coli* free of adsorbed nanoparticles. A higher OD value of the supernatant indicates a lower adsorption of nanoparticles on the bacterial surface. From Figure 8a, one can see that ZnO/GQD−PEI(6×) exhibited more extensive adsorption onto the bacterial surface than ZnO/GQD and more adsorption at longer mixing time, in comparison to the control experiment.

The disparity of the adsorption of nanocomposites onto bacterial cells can be accounted for by their ζ-potentials. It can be seen that *E. coli* in water showed a ζ-potential of −25.7 mV, indicating that the cell surface was largely negatively charged (Figure 8b). ZnO/GQD also exhibited a negative ζ-potential (−40.4 mV), likely due to a large number of negatively charged oxygenated groups on the GQD surface.[29] By contrast, the ζ-potential of ZnO/GQD−PEI(6×) nanocomposite was actually positive at +16.67 mV (Figure 8d) due to the cationic PEI that possessed positively charged $-NH_2^+-$ moieties, which led to strong adsorption onto the negatively charged bacteria.[49]

Solution pH was found to play a critical role in determining the ζ-potential and hence the adsorption of nanocomposites onto the bacterial cells (Figure S4, SI) and the antibacterial properties of the nanocomposites (Figure S5, SI). As shown in Figure S5 (SI), a larger number of *E. coli* remained after the

DOI: 10.1021/acssuschemeng.9b03292
ACS Sustainable Chem. Eng. 2019, 7, 16264−16273

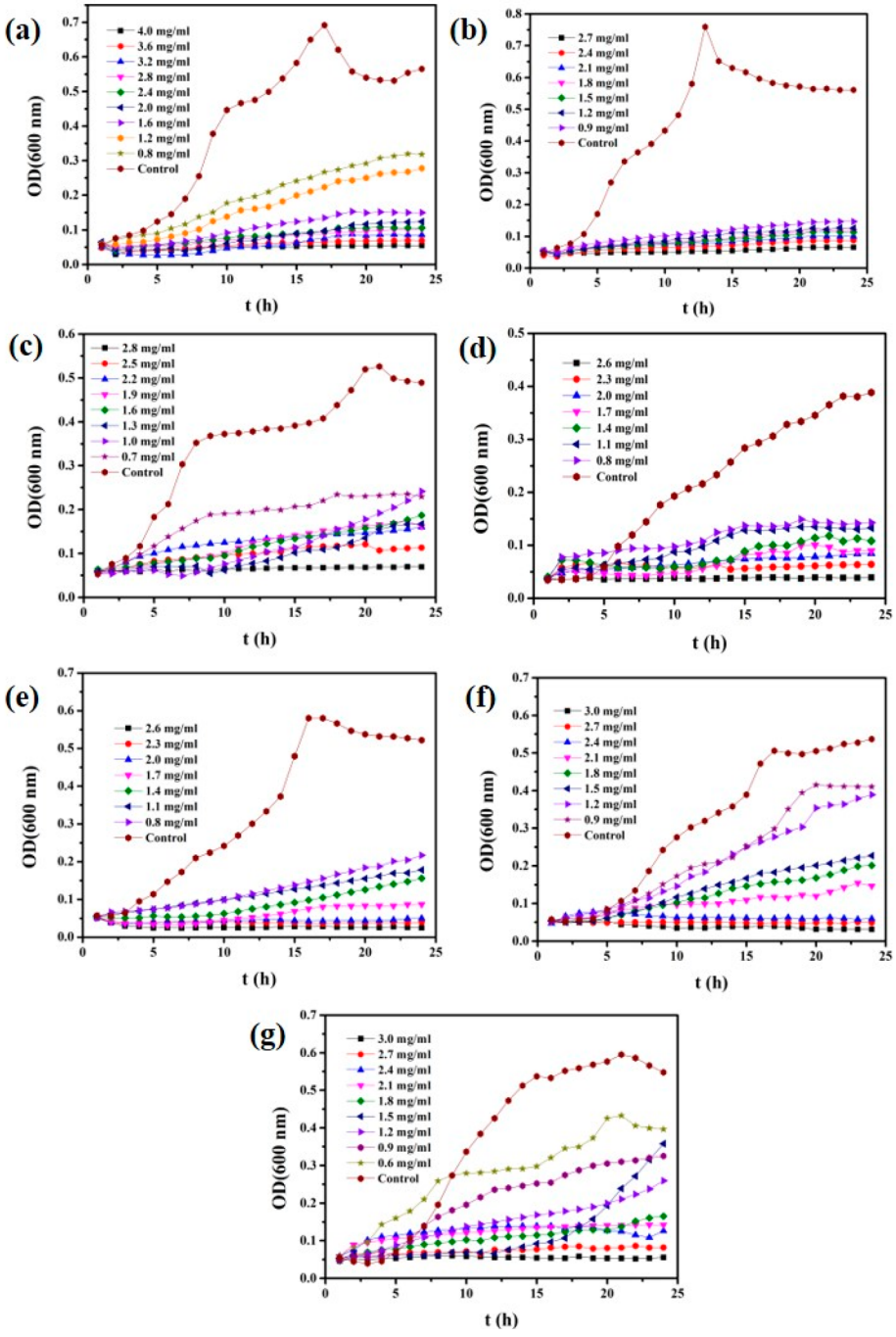

Figure 5. Growth curves of *E. coli* in nutritional broth containing (a) ZnO/GQD and various ZnO/GQD−PEI nanocomposites for 24 h under ambient conditions: (b) ZnO/GQD−PEI(1×), (c) ZnO/GQD−PEI(2×), (d) ZnO/GQD−PEI(4×), (e) ZnO/GQD−PEI(6×), (f) ZnO/GQD−PEI(8×), and (g) ZnO/GQD−PEI(10×).

treatment of ZnO/GQD−PEI(6×) nanocomposite than after that of ZnO/GQD in either more acidic (pH 3) or more alkaline (pH 11) media. It was probably due to a change of the ζ-potential of the ZnO/GQD−PEI(6×) nanocomposite to +7.36 mV at pH 3 and −14.4 mV at pH 11 that diminished the adsorption onto the negatively charged bacteria, as displayed in Figure S4 (SI). Taken together, these results suggest that modification of nanocomposites with cationic polymers can be an effective strategy to enhance the interactions with negatively charged bacteria.[50−52]

The morphology of the *E. coli* cells after nanocomposite treatment was also examined by TEM measurements. Figure 9 shows the TEM images of the bacterial cells after treatment with ZnO/GQD or ZnO/GQD−PEI(6×) for 10 h under ambient conditions. It can be observed that there are numerous bacteria cells with a regular morphology and a smooth surface in the control group of untreated *E. coli* (Figure 9a). By contrast, the number of *E. coli* cells decreased markedly, and the cell membranes were apparently damaged after the treatment with ZnO/GQD and ZnO/GQD−PEI(6×) nanocomposites (Figure 9b,c). Because of large-scale leakage of proteins and cytoplasm from the ruptured *E. coli* cells, the color of the bacterial cells became light gray, in comparison with the dark black color in the control group.

DOI: 10.1021/acssuschemeng.9b03292
ACS Sustainable Chem. Eng. 2019, 7, 16264−16273

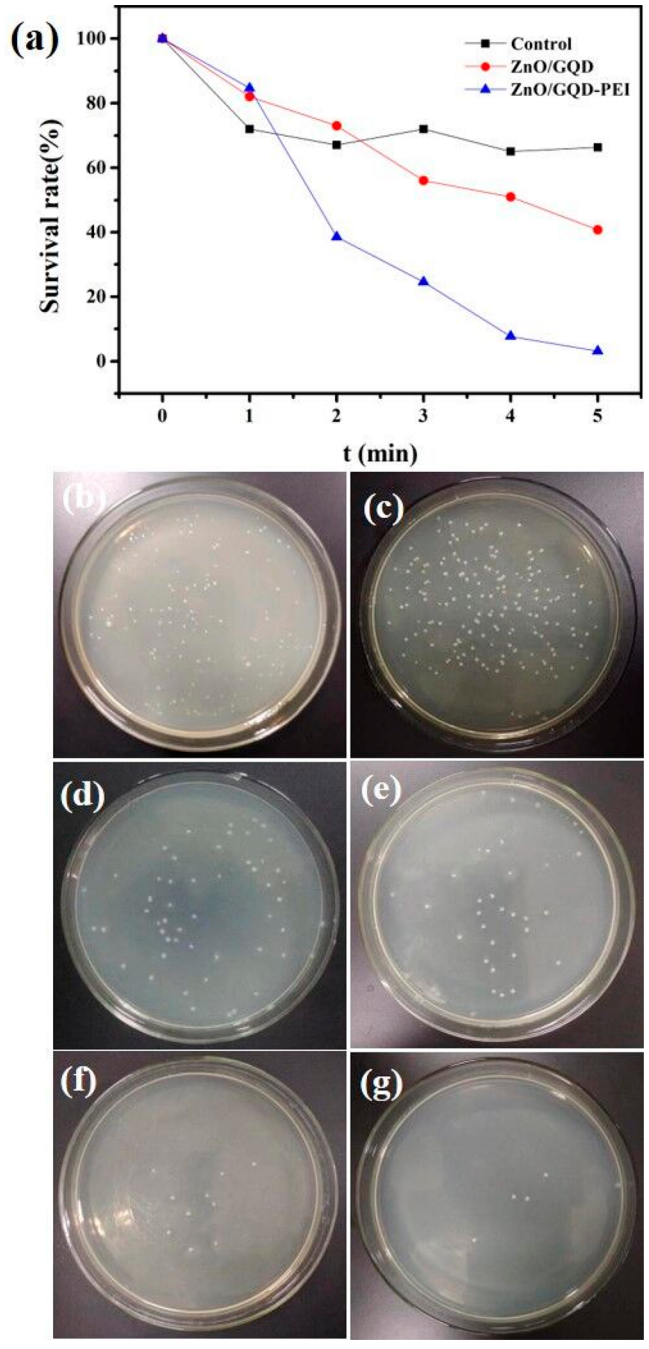

Figure 6. (a) Survival rate of *E. coli* treated with ZnO/GQD and ZnO/GQD−PEI(6×) nanocomposites under UV irradiation for different periods of time. Digital images of *E. coli* after the treatment with ZnO/GQD−PEI(6×) nanocomposites under UV irradiation for different periods of time: (b) 0 min, (c) 1 min, (d) 2 min, (e) 3 min, (f) 4 min, and (g) 5 min.

Additionally, obvious apoptosis of bacterial cells also occurred after exposure to ZnO/GQD and ZnO/GQD−PEI(6×) nanocomposites. It should be noted that ZnO/GQD agglomerated significantly in the treatment of *E. coli* (Figure 9b,e). However, the ZnO/GQD−PEI(6×) nanocomposite was adsorbed rather uniformly around the cells, with some even inside the cells (Figure 9c,f), resulting in a significantly lower number of residual cells than with ZnO/GQD. This further confirms the superior antibacterial activities of the ZnO/GQD−PEI nanocomposites. Therefore, the high antibacterial

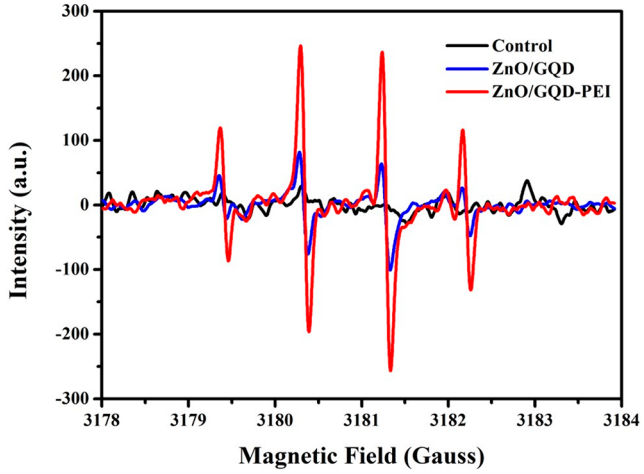

Figure 7. ESR spectra of blank water and dispersions of ZnO/GQD and ZnO/GQD−PEI(6×) nanocomposites under ambient conditions.

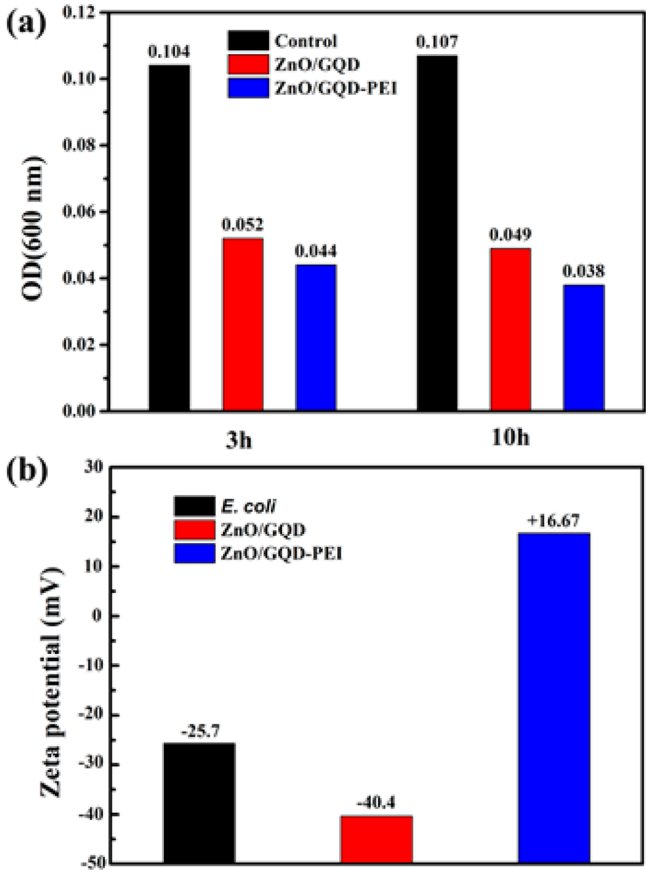

Figure 8. (a) *E. coli* concentration after adsorption of the ZnO/GQD and ZnO/GQD−PEI(6×) nanocomposites for 3 h and (b) ζ-potentials of *E. coli*, ZnO/GQD, and ZnO/GQD−PEI(6×) nanocomposites.

activity of ZnO/GQD−PEI nanocomposites was most likely due to the enhanced dispersion of the nanocomposites by PEI capping and the resulting electrostatic attraction with target bacteria, leading to apparent membrane damage. In addition, the increased ROS level by photoirradiation of the nanocomposites (Figure 7) resulted in effective apoptosis of bacterial cells.

DOI: 10.1021/acssuschemeng.9b03292
ACS Sustainable Chem. Eng. 2019, 7, 16264−16273

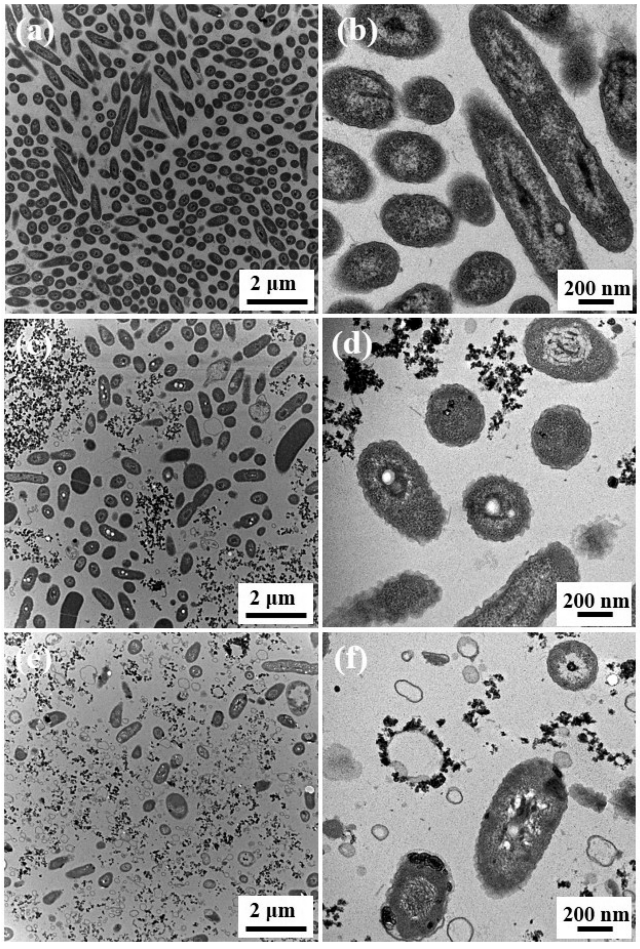

Figure 9. Structural changes of (a, d) untreated *E. coli* cells and *E. coli* cells after the treatment of (b, e) ZnO/GQD nanocomposites and (c, f) ZnO/GQD−PEI nanocomposites.

The antibacterial process of ZnO/GQD−PEI nanocomposites against *E. coli* is schematically illustrated in Figure 10. First, the capping of PEI enhances the dispersibility of the nanocomposites in water and the strong electrostatic attractions facilitate the adsorption of the ZnO/GQD−PEI nanocomposites onto the bacterial cell surface. The cytomembranes try to maintain the original surface charge by extricating the attached nanoparticles through endocytosis. During this process, both the rigidity and morphology of the cytomembrane can be changed.[51] Additionally, with the accumulation of ZnO/GQD−PEI nanocomposites on the cell surface, the physical mobility of the cell membrane is impeded, which can lead to membrane damage and cytoplasmic leakage.[53] The release of Zn^{2+} ions and the formation of ROS by the photochemical reactivity of ZnO/GQD−PEI nanocomposites can occur both inside and outside of the bacterial cells, which may interact with nucleic acids and proteins in the *E. coli* cells, thereby resulting in the eventual cell death.[54]

CONCLUSION

In this study, uniformly dispersed ZnO/GQD−PEI nanocomposites were successfully synthesized by a sol−gel method and exhibited a significantly improved antibacterial property toward *E. coli* under ambient conditions, as compared to the ZnO/GQD counterpart. This is ascribed to the synergistic interactions among the three structural constituents, where

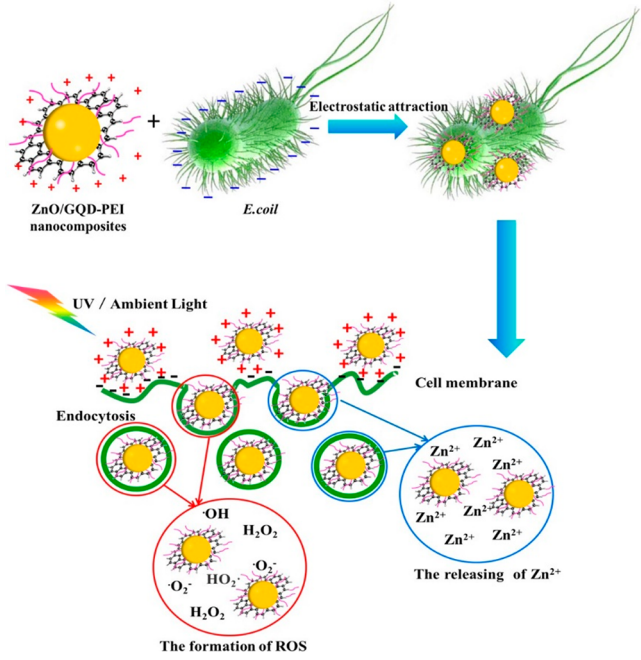

Figure 10. Schematic of the antibacterial process of ZnO/GQD−PEI nanocomposites against *E. coli*.

ZnO is the main antibacterial ingredient, interfacial charge transfer from GQD to ZnO facilitates the generation of hydroxyl radicals, and PEI improves the dispersion and adsorption of the nanocomposites onto the bacterial cells, primarily due to electrostatic interactions. Results from the work suggest that deliberate engineering of functional nanocomposites may lead to marked enhancement of the antibacterial performance.

ASSOCIATED CONTENT

Supporting Information

The Supporting Information is available free of charge on the ACS Publications website at DOI: 10.1021/acssuschemeng.9b03292.

Additional experimental data (Figures S1−S5 and Table S1) (PDF)

AUTHOR INFORMATION

Corresponding Authors

*J.L. e-mail: liujunli042@163.com.

*S.C. e-mail: shaowei@ucsc.edu

ORCID

Hui Liu: 0000-0002-5966-1191

Aiqin Wang: 0000-0002-9963-7460

Shaowei Chen: 0000-0002-3668-8551

Author Contributions

The manuscript was written through contributions of all authors. All authors have given approval to the final version of the manuscript.

Notes

The authors declare no competing financial interest.

ACKNOWLEDGMENTS

This investigation was supported by the National Natural Science Foundation of China for Young Scholar (51802185),

DOI: 10.1021/acssuschemeng.9b03292
ACS Sustainable Chem. Eng. 2019, 7, 16264−16273

the Key Laboratory of Clay Mineral Applied Research of Gansu Province (CMAR-2017-03), the China Postdoctoral Science Foundation (2018M643558), the R&D Center of Xuyi Palygorskite Applied Technology Lanzhou Institute of Chemical Physics Chinese Academy of Sciences (LICP-XY2019-01). S.C. thanks the National Science Foundation for partial support of the work (CHE-1710408 and CBET-1848841).

REFERENCES

(1) Morens, D. M.; Folkers, G. K.; Fauci, A. S. The challenge of emerging and re-emerging infectious diseases. *Nature* **2004**, *430*, 242−249.
(2) Chen, S.; Quan, Y.; Yu, Y. L.; Wang, J. H. Graphene Quantum Dot/Silver Nanoparticle Hybrids with Oxidase Activities for Antibacterial Application. *ACS Biomater. Sci. Eng.* **2017**, *3*, 313−321.
(3) Dunlop, P. S. M.; Byrne, J. A.; Manga, N.; Eggins, B. R. The photocatalytic removal of bacterial pollutants from drinking water. *J. Photochem. Photobiol., A* **2002**, *148*, 355−363.
(4) Huang, W. J.; Fang, G. C.; Wang, C. C. The determination and fate of disinfection by-products from ozonation of polluted raw water. *Sci. Total Environ.* **2005**, *345*, 261−272.
(5) Robertson, J. M. C.; Robertson, P. K. J.; Lawton, L. A. A comparison of the effectiveness of TiO_2 photocatalysis and UVA photolysis for the destruction of three pathogenic micro-organisms. *J. Photochem. Photobiol., A* **2005**, *175*, 51−56.
(6) Rojas-Andrade, M. D.; Chata, G.; Rouholiman, D.; Liu, J.; Saltikov, C.; Chen, S. Antibacterial mechanisms of graphene-based composite nanomaterials. *Nanoscale* **2017**, *9*, 994−1006.
(7) Talebian, N.; Amininezhad, S. M.; Doudi, M. Controllable synthesis of ZnO nanoparticles and their morphology-dependent antibacterial and optical properties. *J. Photochem. Photobiol., B* **2013**, *120*, 66−73.
(8) Liu, J.; Wang, Y.; Ma, J.; Peng, Y.; Wang, A. A review on bidirectional analogies between the photocatalysis and antibacterial properties of ZnO. *J. Alloys Compd.* **2019**, *783*, 898−918.
(9) Paul, T.; Miller, P. L.; Strathmann, T. J. Visible-light-Mediated TiO_2 photocatalysis of fluoroquinolone antibacterial agents. *Environ. Sci. Technol.* **2007**, *41*, 4720−4727.
(10) Haldorai, Y.; Shim, J.-J. Novel chitosan-TiOnanohybrid: Preparation, characterization, antibacterial, and photocatalytic properties. *Polym. Compos.* **2014**, *35*, 327−333.
(11) Damodar, R. A.; You, S. J.; Chou, H. H. Study the self cleaning, antibacterial and photocatalytic properties of TiO_2 entrapped PVDF membranes. *J. Hazard. Mater.* **2009**, *172*, 1321−1328.
(12) Jiang, Z.; Liang, X.; Liu, Y.; Jing, T.; Wang, Z.; Zhang, X.; Qin, X.; Dai, Y.; Huang, B. Enhancing visible light photocatalytic degradation performance and bactericidal activity of BiOI via ultrathin-layer structure. *Appl. Catal., B* **2017**, *211*, 252−257.
(13) Hui, L.; Huang, J.; Chen, G.; Zhu, Y.; Yang, L. Antibacterial Property of Graphene Quantum Dots (Both Source Material and Bacterial Shape Matter). *ACS Appl. Mater. Interfaces* **2016**, *8*, 20−25.
(14) Ruparelia, J. P.; Chatterjee, A. K.; Duttagupta, S. P.; Mukherji, S. Strain specificity in antimicrobial activity of silver and copper nanoparticles. *Acta Biomater.* **2008**, *4*, 707−716.
(15) Rai, M.; Yadav, A.; Gade, A. Silver nanoparticles as a new generation of antimicrobials. *Biotechnol. Adv.* **2009**, *27*, 76−83.
(16) Gordon, T.; Perlstein, B.; Houbara, O.; Felner, I.; Banin, E.; Margel, S. Synthesis and characterization of zinc/iron oxide composite nanoparticles and their antibacterial properties. *Colloids Surf., A* **2011**, *374*, 1−8.
(17) Tian, J.; Shen, S.; Zhou, C.; Dang, X.; Jiao, Y.; Li, L.; Ding, S.; Li, H. Investigation of the antimicrobial activity and biocompatibility of magnesium alloy coated with HA and antimicrobial peptide. *J. Mater. Sci.: Mater. Med.* **2015**, *26*, 1−12.
(18) Lu, Z.; Rong, K.; Li, J.; Yang, H.; Chen, R. Size-dependent antibacterial activities of silver nanoparticles against oral anaerobic pathogenic bacteria. *J. Mater. Sci.: Mater. Med.* **2013**, *24*, 1465−1471.
(19) Raghupathi, K. R.; Koodali, R. T.; Manna, A. C. Size-dependent bacterial growth inhibition and mechanism of antibacterial activity of zinc oxide nanoparticles. *Langmuir* **2011**, *27*, 4020−4028.
(20) Yoon, K. Y.; Byeon, J. H.; Park, J. H.; Hwang, J. Susceptibility constants of Escherichia coli and Bacillus subtilis to silver and copper nanoparticles. *Sci. Total Environ.* **2007**, *373*, 572−575.
(21) Zhao, R.; Kong, W.; Sun, M.; Yang, Y.; Liu, W.; Lv, M.; Song, S.; Wang, L.; Song, H.; Hao, R. Highly Stable Graphene-Based Nanocomposite (GO−PEI−Ag) with Broad-Spectrum, Long-Term Antimicrobial Activity and Antibiofilm Effects. *ACS Appl. Mater. Interfaces* **2018**, *10*, 17617−17629.
(22) Applerot, G.; Lipovsky, A.; Dror, R.; Perkas, N.; Nitzan, Y.; Lubart, R.; Gedanken, A. Enhanced Antibacterial Activity of Nanocrystalline ZnO Due to Increased ROS-Mediated Cell Injury. *Adv. Funct. Mater.* **2009**, *19*, 842−852.
(23) Li, X.; Lu, Z.; Li, Q. Multilayered films incorporating CdTe quantum dots with tunable optical properties for antibacterial application. *Thin Solid Films* **2013**, *548*, 336−342.
(24) Stankovic, N.; Bodik, M.; Siffalovic, P.; Kotlar, M.; Micusik, M.; Spitalsky, Z.; Danko, M.; Milivojevic, D.; Kleinova, A.; Kubat, P.; et al. Antibacterial and Antibiofouling Properties of Light Triggered Fluorescent Hydrophobic Carbon Quantum Dots Langmuir-Blodgett Thin Films. *ACS Sustainable Chem. Eng.* **2018**, *6*, 4154−4163.
(25) Liu, J.; Rojas-Andrade, M. D.; Chata, G.; Peng, Y.; Roseman, G.; Lu, J. E.; Millhauser, G. L.; Saltikov, C.; Chen, S. Photo-enhanced antibacterial activity of ZnO/graphene quantum dot nanocomposites. *Nanoscale* **2018**, *10*, 158−166.
(26) Stoimenov, P. K.; Klinger, R. L.; Marchin, G. L.; Klabunde, K. J. Metal Oxide Nanoparticles as Bactericidal Agents. *Langmuir* **2002**, *18*, 6679−6686.
(27) An, S. W.; Jeong, Y. C.; Cho, H. H.; Park, J. W. Adsorption of $NH4^+$-N and E. coli onto Mg^{2+}-modified zeolites. *Environ. Earth Sci.* **2016**, *75*, 437.
(28) Zemb, O.; Manefield, M.; Thomas, F.; Jacquet, S. Phage adsorption to bacteria in the light of the electrostatics: A case study using E. coli, T2 and flow cytometry. *J. Virol. Methods* **2013**, *189*, 283−289.
(29) Dong, Y.; Shao, J.; Chen, C.; Li, H.; Wang, R.; Chi, Y.; Lin, X.; Chen, G. Blue luminescent graphene quantum dots and graphene oxide prepared by tuning the carbonization degree of citric acid. *Carbon* **2012**, *50*, 4738−4743.
(30) Yan, L.; Chang, Y.; Zhao, L.; Gu, Z.; Liu, X.; Tian, G.; Zhou, L.; Ren, W.; Jin, S.; Yin, W.; et al. The use of polyethylenimine-modified graphene oxide as a nanocarrier for transferring hydrophobic nanocrystals into water to produce water-dispersible hybrids for use in drug delivery. *Carbon* **2013**, *57*, 120−129.
(31) Son, D. I.; Kwon, B. W.; Park, D. H.; Seo, W.-S.; Yi, Y.; Angadi, B.; Lee, C.-L.; Choi, W. K. Emissive ZnO-graphene quantum dots for white-light-emitting diodes. *Nat. Nanotechnol.* **2012**, *7*, 465−471.
(32) Sakthivel, S.; Neppolian, B.; Shankar, M. V.; Arabindoo, B.; Palanichamy, M.; Murugesan, V. Solar photocatalytic degradation of azo dye: comparison of photocatalytic efficiency of ZnO and TiO_2. *Sol. Energy Mater. Sol. Cells* **2003**, *77*, 65−82.
(33) Valles, C.; Drummond, C.; Saadaoui, H.; Furtado, C. A.; He, M.; Roubeau, O.; Ortolani, L.; Monthioux, M.; Penicaud, A. Solutions of negatively charged graphene sheets and ribbons. *J. Am. Chem. Soc.* **2008**, *130*, 15802−15804.
(34) Dhar, S.; Majumder, T.; Mondal, S. P. Graphene Quantum Dot-Sensitized ZnO Nanorod/Polymer Schottky Junction UV Detector with Superior External Quantum Efficiency, Detectivity, and Responsivity. *ACS Appl. Mater. Interfaces* **2016**, *8*, 31822−31831.
(35) Singhal, A.; Achary, S. N.; Manjanna, J.; Chatterjee, S.; Ayyub, P.; Tyagi, A. K. Chemical Synthesis and Structural and Magnetic Properties of Dispersible Cobalt-and Nickel-Doped ZnO Nanocrystals. *J. Phys. Chem. C* **2010**, *114*, 3422−3430.
(36) Kumar, R.; Anandan, S.; Hembram, K.; Rao, T. N. Efficient ZnO-based visible-light-driven photocatalyst for antibacterial applications. *ACS Appl. Mater. Interfaces* **2014**, *6*, 13138−13148.

DOI: 10.1021/acssuschemeng.9b03292
ACS Sustainable Chem. Eng. 2019, 7, 16264−16273

(37) Cai, A.; Wang, X.; Qi, Y.; Ma, Z. Hierarchical ZnO/S,N:GQD composites: Biotemplated synthesis and enhanced visible-light-driven photocatalytic activity. *Appl. Surf. Sci.* **2017**, *391*, 484−490.
(38) Vanzetti, L.; Pasquardini, L.; Potrich, C.; Vaghi, V.; Battista, E.; Causa, F.; Pederzolli, C. XPS analysis of genomic DNA adsorbed on PEI-modified surfaces. *Surf. Interface Anal.* **2016**, *48*, 611−615.
(39) Tayyebi, A.; Outokesh, M.; Tayebi, M.; Shafikhani, A.; Şengör, S. S. ZnO quantum dots-graphene composites: Formation mechanism and enhanced photocatalytic activity for degradation of methyl orange dye. *J. Alloys Compd.* **2016**, *663*, 738−749.
(40) Xu, T.; Zhang, L.; Cheng, H.; Zhu, Y. Significantly enhanced photocatalytic performance of ZnO via graphene hybridization and the mechanism study. *Appl. Catal., B* **2011**, *101*, 382−387.
(41) Chang, H.; Sun, Z.; Ho, K. Y.-F.; Tao, X.; Yan, F.; Kwok, W.-M.; Zheng, Z. A highly sensitive ultraviolet sensor based on a facile in situ solution-grown ZnO nanorod/graphene heterostructure. *Nanoscale* **2011**, *3*, 258−264.
(42) Muhl, S.; Méndez, J. M. A review of the preparation of carbon nitride films. *Diamond Relat. Mater.* **1999**, *8*, 1809−1830.
(43) Luo, J.; Jiang, S.; Liu, X. Efficient One-Pot Synthesis of Mussel-Inspired Molecularly Imprinted Polymer Coated Graphene for Protein-Specific Recognition and Fast Separation. *J. Phys. Chem. C* **2013**, *117*, 18448−18456.
(44) Buchman, Y. K.; Lellouche, E.; Zigdon, S.; Bechor, M.; Michaeli, S.; Lellouche, J. P. Silica nanoparticles and polyethyleneimine (PEI)-mediated functionalization: a new method of PEI covalent attachment for siRNA delivery applications. *Bioconjugate Chem.* **2013**, *24*, 2076−2087.
(45) Lo, C. W.; Liao, W. H.; Wu, C. H.; Lee, J. L.; Sun, M. K.; Yang, H. S.; Tsai, W. B.; Chang, Y.; Chen, W. S. Synergistic Effect of PEI and PDMAEMA on Transgene Expression in Vitro. *Langmuir* **2015**, *31*, 6130−6136.
(46) Serpone, N.; Texier, I.; Emeline, A. V.; Pichat, P.; Hidaka, H.; Zhao, J. Post-irradiation effect and reductive dechlorination of chlorophenols at oxygen-free TiO_2/water interfaces in the presence of prominent hole scavengers. *J. Photochem. Photobiol., A* **2000**, *136*, 145−155.
(47) Kokorin, A. I.; Patsevich, I. V.; Fridman, A. I.; Shlapnikova, N. L. EPR study of rhodium complexes with polyethyleneimine. *Bull. Acad. Sci. USSR, Div. Chem. Sci.* **1986**, *35*, 1613−1618.
(48) Dubose, C. M.; Rehorek, D.; Oehler, U. M.; Janzen, E. G. Spin trapping: ESR parameters of spin adducts. *Free Radic. Biol. Med.* **1988**, *5*, 55−56.
(49) Chen, Z.; Zhang, L.; He, Y.; Li, Y. Sandwich-type Au-PEI/DNA/PEI-Dexa nanocomplex for nucleus-targeted gene delivery in vitro and in vivo. *ACS Appl. Mater. Interfaces* **2014**, *6*, 14196−14206.
(50) Ge, S.; Agbakpe, M.; Zhang, W.; Kuang, L. Heteroaggregation between PEI-coated magnetic nanoparticles and algae: effect of particle size on algal harvesting efficiency. *ACS Appl. Mater. Interfaces* **2015**, *7*, 6102−6108.
(51) Cho, E. C.; Xie, J.; Wurm, P. A.; Xia, Y. Understanding the role of surface charges in cellular adsorption versus internalization by selectively removing gold nanoparticles on the cell surface with a I_2/KI etchant. *Nano Lett.* **2009**, *9*, 1080−1084.
(52) Israel, L. L.; Lellouche, E.; Ostrovsky, S.; Yarmiayev, V.; Bechor, M.; Michaeli, S.; Lellouche, J. P. Acute in vivo toxicity mitigation of PEI-coated maghemite nanoparticles using controlled oxidation and surface modifications toward siRNA delivery. *ACS Appl. Mater. Interfaces* **2015**, *7*, 15240−15255.
(53) Zhao, R.; Lv, M.; Li, Y.; Sun, M.; Kong, W.; Wang, L.; Song, S.; Fan, C.; Jia, L.; Qiu, S.; et al. Stable Nanocomposite Based on PEGylated and Silver Nanoparticles Loaded Graphene Oxide for Long-Term Antibacterial Activity. *ACS Appl. Mater. Interfaces* **2017**, *9*, 15328−15341.
(54) Ma, J.; Liu, J.; Bao, Y.; Zhu, Z.; Wang, X.; Zhang, J. Synthesis of large-scale uniform mulberry-like ZnO particles with microwave hydrothermal method and its antibacterial property. *Ceram. Int.* **2013**, *39*, 2803−2810.

DOI: 10.1021/acssuschemeng.9b03292
ACS Sustainable Chem. Eng. 2019, 7, 16264−16273